Variable Nature of Magnetically-Driven Ultra-Fast Outflows

Keigo Fukumura[1], Demosthenes Kazanas[2], Chris Shrader[2,3], Ehud Behar[4], Francesco Tombesi[2,5,6] and Ioannis Contopoulos[7]

August 28, 2018

Received _____; accepted _____

[1]Department of Physics and Astronomy, James Madison University, Harrisonburg, VA 22807; fukumukx@jmu.edu

[2]Astrophysics Science Division, NASA/Goddard Space Flight Center, Greenbelt, MD 20771

[3]Catholic University of America, Washington, DC 20064

[4]Department of Physics, Technion, Haifa 32000, Israel

[5]Department of Astronomy and CRESST, University of Maryland, College Park, MD20742

[6]Department of Physics, University of Rome "Tor Vergata", Via della Ricerca Scientifica 1, I-00133 Rome, Italy

[7]Research Center for Astronomy, Academy of Athens, Athens 11527, Greece

ABSTRACT

Among a number of active galactic nuclei (AGNs) that drive ionized outflows in X-rays, a low-redshift ($z = 0.184$) quasar, PDS 456, is long known to exhibit one of the exemplary ultra-fast outflows (UFOs). However, the physical process of acceleration mechanism is yet to be definitively constrained. In this work, we model the variations of the Fe K UFO properties in PDS 456 over many epochs in X-ray observations in the context of magnetohydrodynamic (MHD) accretion-disk winds employed in our earlier studies of similar X-ray absorbers. We applied the model to the 2013/2014 *XMM-Newton*/*NuSTAR* spectra to determine the UFO's condition; namely, velocity, ionization parameter, column density and equivalent width (EW). Under some provisions on the dependence of X-ray luminosity on the accretion rate applicable to near-Eddington state, our photoionization calculations, coupled to a 2.5-dimensional MHD-driven wind model, can further reproduce the observed correlations of the UFO velocity and the anti-correlation of its EW with X-ray strength of PDS 456. This work demonstrates that UFOs, even without radiative pressure, can be driven as an extreme case purely by magnetic interaction while also producing the observed spectrum and correlations.

Subject headings: accretion, accretion disks — (galaxies:) quasars: absorption lines — methods: numerical — galaxies: individual (PDS 456) — magnetohydrodynamics (MHD)

1. Introduction

One of the generic features seen in black hole (BH) systems such as active galactic nuclei (AGNs) and Galactic X-ray binaries (XRBs) are blue-shifted absorption features in their spectra primarily detected in the UV and the X-ray bands, with the latter also known as warm absorbers (WAs). Within the last decade, on the other hand, a new class of outflows has drawn much attention because of their unique physical characteristics: They are ejected at near-relativistic velocities ($v/c \sim 0.1 - 0.7$), with nearly Compton-thick columns ($10^{23} \lesssim N_H \lesssim 10^{24}$ cm^{-2}) and systematically high ionization parameter[1] ($\log \xi \sim 4 - 6$). These ultra-fast outflows (UFOs), primarily observed with high-throughput CCD detectors, appear to be present not only in nearby Seyfert AGNs (e.g. Tombesi et al. 2010, 2011, 2014) but also in very bright (lensed) quasars (e.g. Chartas et al. 2003; Pounds et al. 2003; Chartas et al. 2009a; Dadina et al. 2018) and presumably in the ultraluminous X-ray sources (e.g. Walton et al. 2016). While WA/UFO signatures in the X-ray spectra are thought to be generic to accretion-powered sources, their launching mechanism is still poorly understood.

PDS 456 is an archetypal nearby ($z = 0.184$), radio-quiet quasar (QSO) hosting a BH of mass $M \sim 10^9 M_\odot$ (e.g. Reeves et al. 2009), being the most luminous AGN in the local universe with a bolometric luminosity of $L_{\rm bol} \sim 10^{47}$ erg/s. It is among the best studied QSOs for its strong UFO signatures observed in the Fe K band in the past X-ray observations with *Suzaku* (e.g. Reeves et al. 2009, 2014; Gofford et al. 2014; Matzeu et al. 2016), *XMM-Newton*/EPIC and *NuSTAR* (e.g. Reeves et al. 2003; Behar et al. 2010; Nardini et al. 2015, hereafter, N15). A number of these extensive monitoring campaigns of PDS 456 at different flux levels between 2001 and 2014 has provided us with insights into the variable nature of the UFOs since its first discovery (e.g. Reeves et al. 2003). Detailed spectral analyses have consistently confirmed that the highly ionized UFOs of $v/c \sim 0.2 - 0.3$ could be identified as the 1s-2p resonance transitions of Fe XXVI with almost Compton-thick column of $N_H \lesssim 10^{24}$ cm^{-2} and high ionization parameter of $\log \xi \sim 4 - 6$ (e.g. Reeves et al. 2009). The distance of the observed UFOs is estimated to lie within $\sim 50 R_S$ where R_S is the Schwarzschild radius (e.g. Reeves et al. 2009). The spectral variability has been studied as well suggesting that variable partial covering and/or intrinsic continuum variation may cause the observed short-term variability in X-ray (Matzeu et al. 2016, hereafter, M16). Reeves et al. (2018) also found an even faster Fe K UFO ($v/c \sim 0.42$) in 2017 *XMM-Newton/NuSTAR* observation.

The QSO outflows have been thought to be driven by radiation pressure by their

[1]This is defined as $\xi \equiv L_{\rm ion}/(nr^2)$ where $L_{\rm ion}$ is ionizing (X-ray) luminosity, n is plasma number density at distance r from the BH.

O/UV flux, in a manner similar to that observed in massive stars (King 2010; Hagino et al. 2015; King & Pounds 2015; Hagino et al. 2017; Nomura & Ohsuga 2017). However, most UFOs are so highly ionized that there is little UV or soft X-ray opacity, making this process very inefficient (e.g. Higginbottom et al. 2014). Alternatively, winds can be driven by the action of global magnetic fields threading the accretion disk to provide a plausible means of efficient acceleration as observed (e.g. Blandford & Payne 1982, hereafter, BP82; Contopoulos & Lovelace 1994, hereafter, CL94; Köngl & Kartje 1994, Fukumura et al. 2010a, hereafter F10; Kazanas et al. 2012; Kazanas 2015; Kraemer et al. 2018).

PDS 456 UFOs are especially interesting because of the variation of its properties with the X-ray variability over the past fifteen or so years. For example, Matzeu et al. (2017, hereafter, M17) noted, over a decade of multi-epoch observations, that the detected Fe K UFO velocity is well correlated with X-ray luminosity L_X $(7-30$ keV) suggestive of a radiative-driven origin. Independently, Parker et al. (2018, hereafter, Pa18) showed a likely anti-correlation between the observed UFO EW and $2-10$ keV flux. A similar trend is also reported in the *XMM-Newton*/EPIC-pn and *NuSTAR* spectra for the low-redshift narrow-line Seyfert 1 (NLS1), IRAS 13224-3809 (Parker et al. 2017, hereafter P17; Pinto et al. 2018, hereafter Pi18) possibly accreting at near-Eddington rate.

Motivated by these findings, we investigate in this Letter the dependence of the variation of the UFO properties on the X-ray flux within the MHD wind framework of our earlier studies. In §2, we overview the proposed wind models. In §3, we present our results and demonstrate that magnetically-driven winds can account for the observed correlations. In §4 we conclude with a summary and discussion.

2. MHD-Driven Wind Model

The magnetically-launched disk-wind model has been applied to account successfully for the X-ray absorber properties of sources of very wide mass range; i.e. the galactic XRB GRO J1655-40 (Fukumura et al. 2017) to the Seyfert 1 NGC 3783 (Fukumura et al. 2018) and a nearby QSO, PG 1211+143 (Fukumura et al. 2015), thus establishing its scale-invariance with BH mass and its broad applicability. **A detailed model description can be found in the above references and we will briefly review the essential elements of the model below.**

PDS 456, because of its very high accretion rate, may present an uncertainty in relating the ionizing luminosity $L_{\rm ion}$ (13.6 eV - 13.6 keV) to the mass-accretion rate $\dot{m}_a$, provided by its large O/UV luminosity. We thus parameterize this as $L_{\rm ion} \equiv f_{44} 10^{44}$ erg s^{-1} such that $f_{44} \propto \dot{m}_a^s$ with $s < 1$ since a part of the radiation is likely to be trapped in the flow and advected into the BH for $\dot{m}_a \gtrsim 1$ (e.g. Takeuchi et al. 2009, for supercritical accretion). We

introduce the fractional mass outflow rate to mass accretion rate, η_w, such that $\eta_w \propto \dot{m}_a$ rather than being constant, allowing the wind mass flux to vary. The wind density is given by $n_w(r,\theta) = n_o^w (r/R_S)^{-p} g(\theta)$ where n_o^w denotes the wind density normalization (i.e. wind density at its innermost launching radius on the disk surface at $r \gtrsim R_S$), with the index $p = 1.2$ observationally consistent with our earlier work (Behar 2009; Fukumura et al. 2017, 2018) . Note that $g(\theta)$ is the (polar) angular dependence **to be solved by the model (see CL94, F10)**. Since the plasma optical depth on the disk surface is proportional to $\sigma_T R_S n_o$ where σ_T is the Thomson cross section, it is found that

$$n_o \sim \frac{\tau}{\sigma_T R_S} \propto \frac{\dot{m}_a}{\sigma_T R_S} \ , \quad n_o^w \sim \frac{\eta_w \dot{m}_a}{\sigma_T R_S} \ . \tag{1}$$

One can then express $\dot{m}_a$ in terms of f_{44} to yield $n_o^w \propto \eta_w \dot{m}_a \propto \dot{m}_a^2 \propto f_{44}^{2/s} \equiv n_{10} 10^{10}$ cm^{-3} where n_{10} is to be constrained by observations. Hence, the ionization parameter ξ scales with f_{44} as $\xi \propto f_{44}/n_o^w \propto f_{44}^{1-2/s}$. With this scalings the wind density increases faster than the X-ray flux for $s < 2$, and therefore, increase in $L_{\rm ion}$ will bring the wind ionization front to smaller radii, yielding higher plasma velocities.

While the wind kinematics is fully determined by the ideal MHD equations (e.g. BP82, Köngl & Kartje 1994, CL94, Kraemer et al. 2018), we consider a possibility of truncated disk, as often discussed (e.g. Nemmen et al. 2014; Hogg & Reynolds 2018), by introducing an **inner truncation launching radius**, R_T. **This parameter is constrained by fitting the observed UFO spectrum.** Given the presence of the big-blue-bump (generally attributed to the accretion disk; see, Matzeu et al. 2016), we assume a fiducial value of $\theta_{\rm obs} = 50^\circ$ for the inclination angle, as also previously suggested (e.g. Reeves et al. 2009, 2014; Hagino et al. 2015). **It should be kept in mind that no radiation is deliberately taken into account in this work to illustrate the pure magnetic case.**

Employing the self-similar prescription in the radial direction with the Keplerian velocity profile ($v \propto r^{-1/2}$), the poloidal field structure is determined by numerically solving the Grad-Shafranov equation as is originally formulated in CL94. Hence, the wind geometry is inherently 2.5D. The outflowing plasma is then photoionized by the radiation of spectral shape F_ν and luminosity $L_{\rm ion}$ assumed to be a compact region much smaller than the UV-emitting region (e.g. Chartas et al. 2009b; Morgan et al. 2012). We adopt the input SED of PDS 456 from M16 where simultaneous observations with *XMM-Newton*/OM and *NuSTAR* in 2014 are phenomenologically parameterized in a double broken power-law form; i.e. $\Gamma = 0.7$ for O/UV - 10 eV, $\Gamma = 3.3$ for soft X-ray band and $\Gamma = 2.4$ beyond 0.5 keV (see also N15).

In response to the irradiating SED, the wind ionization is computed as described in F10, by employing `xstar` (Kallman & Bautista 2001) to calculate the local ionic abundances and the photo-excitation cross section $\sigma_{\rm abs}$. The latter is a function of local wind velocity

$v(r,\theta)$ and its radial shear $v_{\rm shear}(r,\theta)$; the wind shear is implemented in the Voigt function $H(a,u)$ (see F10) to effect a physically motivated local line broadening consistent with the wind kinematics, instead of the arbitrary choice of a *turbulent* velocity (unphysical in its magnitude considering the much smaller thermal plasma velocities). A local line depth is calculated by $\tau_\nu(r,\theta) = \sigma_{\rm abs} N_{\rm ion}$ where $N_{\rm ion}$ is the local ionic column over a discretized small distance Δr ($\Delta r/r = 0.15$) along a line-of-sight (LoS). The observed spectrum is then a superposition of all local spectra over the entire wind (F10). The strength of the UFO feature is measured by equivalent width (EW) as

$$\mathrm{EW}(\theta) \equiv \int_{\rm wind} \left[1 - \prod_{\rm wind} e^{-\tau_\nu(r,\theta)} \right] d\nu \ . \tag{2}$$

3. Results

3.1. UFOs in 2013/2014 Composite Spectrum

We first attempt to model a composite *XMM-Newton/NuSTAR* spectrum in 2013/2014 where these observations were close together in time (4 days) and very little variability is noted. A detailed analysis and discussion are found in N15.

We analyze the spectrum of PDS 456 **by assuming a canonical density slope** $p = 1.2$**, as discussed above.** Adopting the galactic absorption model with `tbabs` where $N_H^{\rm Gal} = 2.4 \times 10^{21}$ cm^{-2} (Kalberla et al. 2005), we initially excluded the Fe K band (~ 7 keV $\lesssim E \lesssim \sim 11$ keV in the rest-frame) to model the underlying continuum, following the earlier analysis by N15. As explained in §2, for a given X-ray luminosity of $f_{44} = 5$ (i.e. $L_{\rm ion} \sim 5 \times 10^{44}$ erg/s) in this specific epoch (Gofford et al. 2014; N15; M17), our primary model parameters include: (1) a wind truncation radius R_T and (2) the density normalization n_{10}, as shown in **Table 1** where we systematically explored the parameter space that yields the bestfit spectrum. To account for the presence of a broad P-Cygni profile at Fe K band (see N15), a single gaussian component `zga` is (phenomenologically) added. With the above continuum, the absorption signature is fitted by our MHD wind model `mhdwind`. This component significantly improves the fit with χ^2/dof=382.8/430 with $R_T/R_S = 7.98^{+0.5}_{-1.2}$ and $n_{10} = 9.1^{+2.8}_{-1.8}$ when $E_{\rm P-Cygni}$ is freely varied, while χ^2/dof=501.1/429 for $R_T/R_S = 7.90^{+0.3}_{-1.5}$ and $n_{10} = 7.6^{+0.46}_{-0.42}$ when fixed at $E_{\rm P-Cygni} = 7.42$ keV as constrained in N15. The former bestfit yields $v_c/c \simeq 0.35$ (the centroid velocity) and $v_{\rm max}/c \simeq 0.39$ (innermost wind velocity). **Figure 1a** shows the *XMM-Newton*/EPIC (black) and *NuSTAR* (red/green) composite spectrum of PDS 456 modeled with the MHD disk-wind (blue) with free $E_{\rm P-Cygni}$. Considering the implied high-velocity and ionization parameter, we only focus on Fe XXVI ion in this work. The Lyβ line, while modeled here, is insignificant due to its lower oscillator strength as expected.

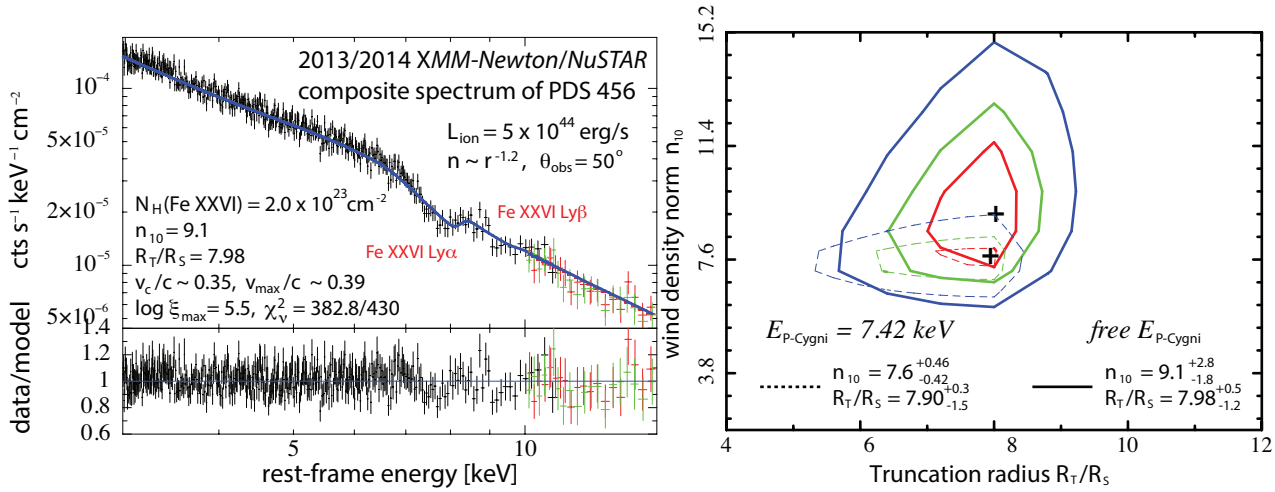

Fig. 1.— (a) A composite *XMM-Newton*/EPIC-pn/mos (black) and *NuSTAR* (red and green) spectrum of PDS 456 (N15) showing the observed Fe K UFOs fitted with the MHD-wind model (blue) with a $p = 1.2$ density profile assuming $\theta_{\rm obs} = 50°$. (b) Confidence contours showing 68% (red), 90% (green) and 99% (blue) levels with the bestfit solution (cross in black) with $E_{\rm P-Cygni} = 7.42$ keV as derived from N15 (dashed) and the *free* $E_{\rm P-Cygni}$ (solid).

A radiative transfer calculation using `xstar` in thermal/ionization equilibrium also provides us with a number of important wind quantities; i.e. the plasma temperature T and ionization parameter ξ and the hydrogen-equivalent column density N_H for the UFO, as listed in **Table 2**. It is seen that the Fe XXVI is formed predominantly in the innermost wind layer close to the truncated radius. The obtained bestfit solution (n_{10}, R_T) is well constrained as demonstrated in the confidence contour in **Figure 1b**. **We note that the bestfit result is almost independent of our choice of $p = 1.2$.** Being encouraged by the successful modeling of the Fe UFO seen in the 2013/2014 data, we then investigate a variable nature of the reported UFO conditions in §3.2.

3.2. The UFO Correlations

Following the successful model fit to the 2013/2014 Fe K UFOs for PDS 456 in §3.1, we investigated the dependence of the UFO properties (i.e. v and EW) on the ionizing

X-ray luminosity depicted by f_{44}, while holding everything else constant for simplicity. It should be reminded that the radiation field plays no role in affecting outflow kinematics in this model. On the other hand, its ionization structure is greatly influenced. As studied in M17, we consider a variable luminosity of $1 \lesssim f_{44} \lesssim 26$ with $\theta = 50°$ assuming that the wind geometry changes very little with changing f_{44} if the underlying global magnetic field is sufficiently "stiff" against the change in radiation field.

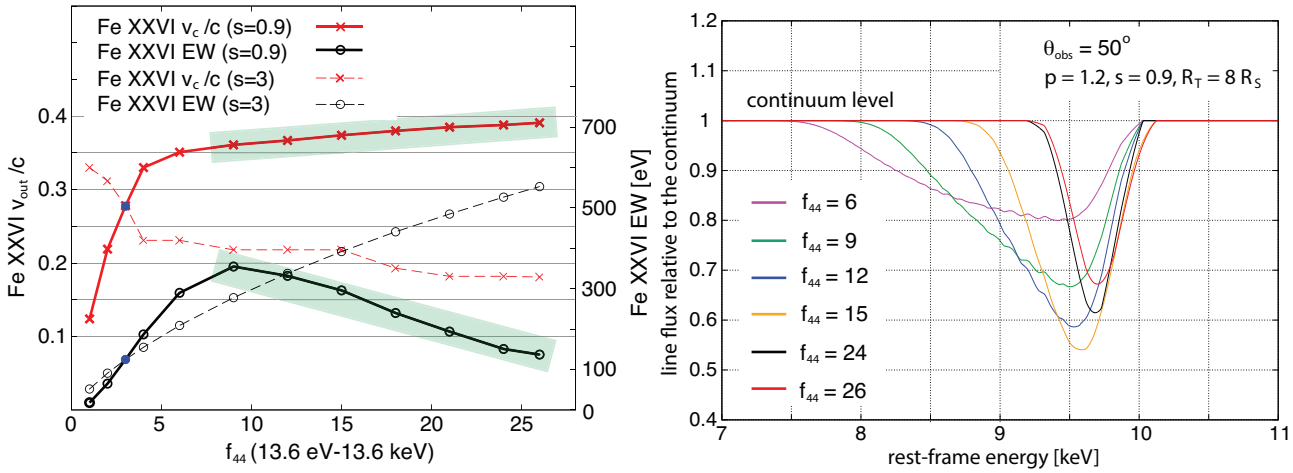

Fig. 2.— (a) An expected correlations between Fe XXVI UFO velocity (red) from the MHD-driven winds as well as the corresponding EW (black) and the broad-band luminosity parameterized as f_{44} for $s = 0.9$ (solid) and $s = 3$ (dashed) scalings. We have used $\theta_{\rm obs} = 50°$ and $p = 1.2$ density profile. The observed correlations are depicted by shaded green region. (b) Predicted template line profiles of Fe XXVI UFOs for different values of f_{44}; 6 (pink), 9 (green), 12 (blue), 15 (orange), 24 (black) and 26 (red) with $\theta = 50°$ for $R_T/R_S = 8$ wind truncation and $p = 1.2$ density profile.

Figure 2a shows the expected correlations of the calculated Fe XXVI centroid velocity v_c/c (red) and its corresponding EW (black) as a function of f_{44} for two cases: $s = 0.9$ (solid) and $s = 3$ (dashed) for comparison. For $s = 0.9$ where wind density increases faster than the X-ray flux with $\dot{m}_a$, it is clearly seen that the velocity is well correlated with f_{44} while its EW is anti-correlated with f_{44} (i.e. X-ray Baldwin effect; Iwasawa & Taniguchi 1993) in a good agreement with data (e.g. M17,P17,Pa18,Pi18). In this case, the UFO location (i.e. ionization front) comes closer to the BH with increasing f_{44} since its radial distance scales as $r_{\rm Fe\,XXVI} \propto \dot{m}_a^{-1/2}$. In contrast, $s = 3$ case is ruled out in this model. We note, for $s = 0.9$, that the predicted Fe XXVI EW exhibits a peak as f_{44} varies due to the

fact that the wind becomes Thomson thick. The exact peak position depends on the SED and the value of s as the wind flux increases with $\dot{m}_a$. Hence, the increasing segment of the EW correlation with is less likely to be observed in near-Eddington sources such as PDS 456 (shaded region in green, consistent with the data), but perhaps it is relevant in low/sub-Eddington Seyferts exhibiting conventional WAs and UFOs.

We show in **Figure 2b** the luminosity-dependence of the predicted Fe XXVI line profiles for $6 \leq f_{44} \leq 26$ with $s = 0.9$. The centroid energy gradually increases with f_{44}, while the line width generally decreases (thus reducing EW) **qualitatively consistent with the multi-epoch *Suzaku* data** (e.g. Matzeu et al. 2016). This can be explained in terms of photoionization of the present model; with increasing $\dot{m}_a$, more plasma is channeled into the wind (i.e. $n_o^w \propto \dot{m}_a^2$ as $\eta_w \propto \dot{m}_a$) from the disk and X-ray power increases as well (i.e. $f_{44} \propto \dot{m}_a^s$). For $\eta_w \propto \dot{m}_a$, the wind density increases faster than the X-ray flux and the the wind ionization parameter ξ slowly decreases with $\dot{m}_a$. **This ionization change will inevitably prevent the wind from producing Fe XXVI as the source brightens. Therefore, only the gas at smaller LoS radius (closer to the irradiating central X-ray source) where velocity is higher can be effectively photoionized to produce Fe XXVI. The dominant heating process for such a large $\dot{m}$ is Compton scattering and electron recoil. Hence, more X-rays are scattered within the near-Compton-thick wind, depleting the photoionizing flux in turn to suppress the efficiency of Fe XXVI production at larger $\dot{m}$.** With further increase in $\dot{m}_a$, this effect becomes more prominent bringing the ionization front more inwards where the wind is faster, while reducing the EW more. These trends are consistent with the multi-epoch observations (M17,Pa18,Pi18). This will eventually lead to little production of Fe XXVI ions resulting in no spectroscopic detection (despite the presence of high-velocity winds at all times).

4. Summary & Discussion

We have employed the MHD accretion disk wind model introduced in our earlier works (F10, F17, F18) to account for the observed correlations of the Fe XXVI UFO in PDS 456. Our model does not include explicitly the effects of radiation pressure, as do models specifically built to consider radiatively-driven outflows (e.g. Higginbottom et al. 2014; Hagino et al. 2017; Nomura & Ohsuga 2017). These are expected to be significant in sources accreting close to their Eddington rate ($\dot{m}_a \simeq 1$) like PDS 456. We have demonstrated by spectral analysis that the observed Fe XXVI UFO feature of PDS 456 can be successfully reproduced within the framework the magnetically-driven disk-winds. Our MHD-wind model can also account for the observed correlations of the UFO velocity and EW with X-ray flux over multi-epoch data. The model assumes that the wind mass flux

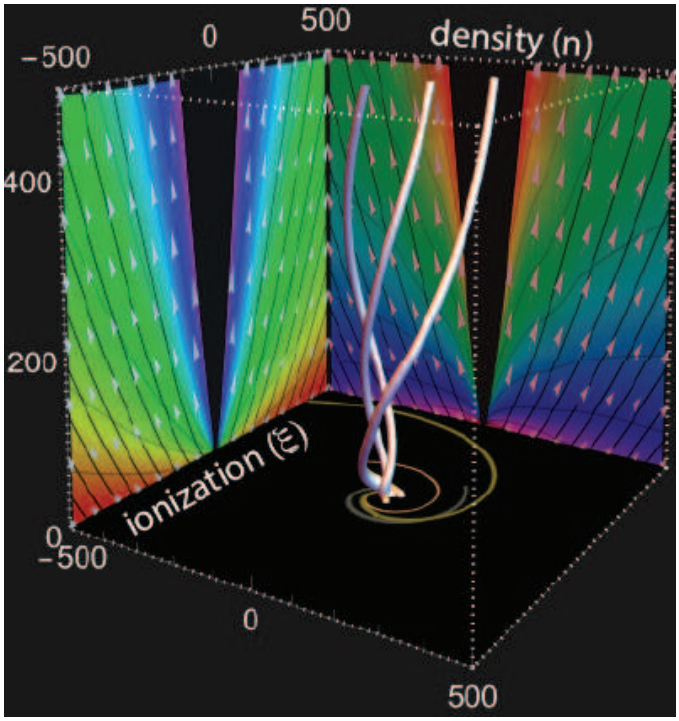

Fig. 3.— Three-dimensional visualization of the calculated streamlines of the wind magnetically launched from a thin disk surface. Wind density $n(r, \theta)$ and fiducial ionization parameter $\xi(r, \theta)$ projected onto the poloidal plane (see F10 for the model description).

can increase faster than X-rays, a situation not unreasonable in such high mass-accretion object where radiation can be trapped and advected with the flow. **Figure 3** shows the calculated streamlines along with wind density $n(r, \theta)$ and fiducial ionization parameter $\xi(r, \theta)$ in the poloidal plane.

The near-Eddington luminosity of PDS 456 is crucial in producing an increase in the UFO velocity with f_{44} since the Fe XXVI velocity is closely related to the local escape velocity. An increase in this velocity implies that the ionization front responsible for the UFO moves radially inwards. This seems natural only when flows are close to Thomson-thick (a fact determined not by the X-rays but by the near-Eddington O/UV luminosity of PDS 456), **which is conceivable as the O/UV photons are closely related to mass-accretion rate**. Of support of this notion are the observations of a near-Eddington narrow-line Seyfert AGN, IRAS 13224-3809, which exhibits similar UFO correlations (Pinto et al. 2018).

To explore this, we have considered different density profiles and confirmed

that the wind of $p = 0.9$ indeed produces a smaller Fe XXVI column (i.e. lower EW) than does the $p = 1.5$ case as discussed in §3.2.

Low/sub-Eddington AGNs to the contrary are not expected to have this effect, allowing the EW to increase with X-ray strength as depicted in **Figure 2a**. **Overall, we note that the exact slope of the calculated correlation is sensitive to the values of s and p as well as the X-ray SED, and the study of such dependences will be left as a future work.**

Fast X-ray outflows have also been detected in BH XRBs (e.g. Miller et al. 2015, 2016) that can be considered as "scaled-down" AGN UFOs in this framework. With timescales much shorter than those in AGNs, fast XRB winds over many binary orbits with X-ray variability may provide us with another valuable clue to systematically understand those correlations as discussed here for PDS 456.

The planned future missions, such as *XARM* and *Athena*, will be able to better constrain the enigmatic UFO properties with unprecedented energy resolution, perhaps leading to answering the ultimate question of its launching mechanism.

We are grateful to the anonymous referee for helpful comments on the original manuscript and James Reeves for providing us with the *XMM-Newton/NuSTAR* spectrum. KF thanks to Alex Sanner for his assistance on wind visualization calculations. This work is supported in part by NASA/ADAP (NNH15ZDA001N-ADAP) and *Chandra* Cycle 17 archive proposal (17700504).

Table 1. Primary Grid of MHD-Wind Model Parameters

Primary Parameter	Value
Truncation radius R_T [in R_S]	$0, 2, 4, 8, 16, 32, 64, 128$
Wind density normalization n_{10}[†]	0.01 - 40

We assume $M = 10^9 M_\odot$ (Reeves et al. 2009), $\theta_{\rm obs} = 50^\circ$ and $p = 1.2$.

[†] Wind density normalization in units of 10^{10} cm^{-3}.

Table 2. Inferred UFO properties with the Best-Fit MHD-Wind Model for 2013/2014 *XMM-Newton*/EPIC and *NuSTAR* Data

Variable	Obtained Value
$E_{\rm P-Cygni}$ [keV]	$6.32^{+0.13}_{-0.25}$ ♯ (7.42; N15) ◇
Density normalization n_{10} † [10^{10} cm^{-3}]	$9.1^{+2.8}_{-1.8}$ ♯ ($7.6^{+0.46}_{-0.42}$) ◇
LoS truncated radius R_T/R_S	$7.98^{+0.5}_{-1.2}$ ($7.90^{+0.3}_{-1.5}$) ◇
Fe XXVI UFO $v_{\rm c}/c$ ♣	0.35
Fe XXVI UFO $v_{\rm max}/c$ ‡	0.39
$\log(\xi_{\rm max}$[erg cm s^{-1}]) ‡	5.5
$\log(T_{\rm max}$[K]) ‡	5.6
N_H(Fe XXVI) [cm^{-2}]	2.0×10^{23}
χ^2/dof	382.8/430 ♯ (501.1/429) ◇

We assume $M = 10^9 M_\odot$ (Reeves et al. 2009), $\theta_{\rm obs} = 50^\circ$ and $p = 1.2$.

† Wind density normalization in units of 10^{10} cm^{-3}.

♣ Calculated value from the modeled centroid velocity.

‡ Calculated value near the truncated radius at $r = R_T$.

♯ Treated as a free parameter.

◇ A fixed value obtained from N15.

REFERENCES

Behar, E., 2009, ApJ, 703, 1346

Behar, E., Kaspi, S., Reeves, J., Turner, T. J., Mushotzky, R., O'Brien, P. T. 2010, ApJ, 712, 26

Blandford, R. D. & Payne, D. G. 1982, MNRAS, 199, 883 (BP82)

Contopoulos, J. & Lovelace, R. V. E. 1994, ApJ, 429, 139 (CL94)

Chartas, G., Brandt, W. N. & Gallagher, S. C. 2003, ApJ, 595, 85

Chartas, G., Saez, C., Brandt, W. N., Giustini, M. & Garmire, G. P. 2009a, ApJ, 706, 644

Chartas, G., Kochanek, C. S., Dai, X., Poindexter, S. & Garmire, G. 2009b, ApJ, 693, 174

Dadina, M., Vignali, C., Cappi, M., Lanzuisi, G., Ponti, G., Torresi, E., De Marco, B., Chartas, G. & Giustini, M. 2018 (arXiv:1801.09839)

Everett, J. E. 2005, ApJ, 631, 689

Fukumura, K., Kazanas, D., Contopoulos, I. & Behar, E. 2010a, ApJ, 715, 636 (F10)

Fukumura, K., Tombesi, F., Kazanas, D., Shrader, C., Behar, E. & Contopoulos, I. 2015, ApJ, 805, 17

Fukumura, K., Kazanas, D., Shrader, C., D., Behar, E., Tombesi, F. & Contopoulos, I. 2017, Nature Astronomy, 1, 0062

Fukumura, K., Kazanas, D., Shrader, C., Behar, E., Tombesi, F. & Contopoulos, I. 2018, ApJ, 853, 40

Gofford, J., Reeves, J. N., Braito, V., Nardini, E., Costa, M. T., Matzeu, G. A., O'Brien, P., Ward, M., Turner, T. J. & Miller, L. 2014, ApJ, 784, 77

Hagino, K., Odaka, H., Done, C., Gandhi, P., Watanabe, S., Sako, M. & Takahashi, T. 2015, MNRAS, 446, 663

Hagino, K., Done, C., Odaka, H., Watanabe, S. & Takahashi, T. 2017, MNRAS, 468, 1442

Higginbottom, N., Proga, D., Knigge, C., Long, K. S., Matthews, J. H. & Sim, S. A. 2014, ApJ, 789, 19

Iwasawa, K. & Taniguchi, Y. 1993, ApJ, 413, L15

Köngl, A. & Kartje, J. F. 1994, ApJ, 434, 446

Hogg, J. D. & Reynolds, C. S. 2018, ApJ, 854, 6

Kalberla, P. M. W., Burton, W. B., Hartmann, D., Arnal, E. M., Bajaja, E., Morras, R. & Pöppel, W. G. L. 2005, A&A, 440, 775

Kazanas, D., Fukumura, K., Contopoulos, I., Behar, E. & Shrader, C. R. 2012, Astronomical Review, 7, 92

Kazanas, D. 2015, ASSL, 414, 207

Kallman, T. & Bautista, M. 2001, ApJS, 133, 221

King, A. R. 2010, MNRAS, 402, 1516

King, A. & Pounds, K. 2015, ARA&A, 53, 115

Köngl, A. & Kartje, J. F. 1994, ApJ, 434, 446

Kraemer, S. B., Tombesi, F. & Bottorff, M. C. 2018, ApJ, 852, 35

Matzeu, G. A., Reeves, J. N., Nardini, E., Braito, V., Costa, M. T., Tombesi, F. & Gofford, J. 2016, MNRAS, 458, 1311

Matzeu, G. A., Reeves, J. N., Braito, V., Nardini, E., McLaughlin, D. E., Lobban, A. P., Tombesi, F. & Costa, M. T. 2017, MNRAS, 472, 15 (M17)

Miller, J. M., Fabian, A. C., Kaastra, J., Kallman, T., King, A. L., Proga, D., Raymond, J. & Reynolds, C. S. 2015, ApJ, 814, 87

Miller, J. M., Raymond, J., Cackett, E., Grinberg, V. & Nowak, M. 2016, ApJ, 822, L18

Morgan, C. W., Hainline, L. J., Chen, B., Tewes, M., Kochanek, C. S., Dai, X., Kozlowski, S., Blackburne, J. A., Mosquera, A. M., Chartas, G., Courbin, F. & Meylan, G. 2012, ApJ, 756, 52

Narayan, R. & Yi, I. 1994, ApJ, 428, L13

Nardini, E. et al. 2015, Science, 347, 860 (N15)

Nemmen, R. S., Storchi-Bergmann, T. & Eracleous, M. 2014, MNRAS, 438, 2804

Nomura, M. & Ohsuga, K. 2017, MNRAS, 465, 2873

Parker, M. L. et al. 2017, Nature, 543, 83 (P17)

Parker, M. L., Reeves, J. N., Matzeu, G. A., Buisson, D. J. K. & Fabian, A. C. 2018, MNRAS, 474, 108 (Pa18)

Pinto, C., Alston, W., Parker, M. L., Fabian, A. C., Gallo, L. C., Buisson, D. J. K., Walton, D. J., Kara, E., Jiang, J., Lohfink, A. & Reynolds, C. S. 2018, MNRAS, 476, 1021 (Pi18)

Pounds, K. A., Reeves, J. N., King, A. R., Page, K. L., O'Brien, P. T. & Turner, M. J. L. 2003, MNRAS, 345, 705

Reeves, J. N., O'Brien, P. T., Braito, V., Behar, E., Miller, L., Turner, T. J., Fabian, A. C., Kaspi, S., Mushotzky, R. & Ward, M. 2009, ApJ, 701, 493

Reeves, J. N., O'Brien, P. T. & Ward, M. J. 2003, ApJ, 593, 65

Reeves, J. N., Braito, V., Gofford, J., Sim, S. A., Behar, E., Costa, M., Kaspi, S., Matzeu, G., Miller, L., O'Brien, P., Turner, T. J. & Ward, M. 2014, ApJ, 780, 45

Reeves, J. N., Braito, V., Nardini, E., Lobban, A. P., Matzeu, G. A. & Costa, M. T. 2018, ApJ, 854, L8

Takeuchi, S., Mineshige, S. & Ohsuga, K. 2009, PASJ, 61, 783

Tombesi, F., Cappi, M., Reeves, J. N., Palumbo, G. G. C., Yaqoob, T., Braito, V. & Dadina, M. 2010, A&A, 521, 57

Tombesi, F., Cappi, M., Reeves, J. N., Palumbo, G. G. C., Braito, V. & Dadina, M. 2011, ApJ, 742, 44

Tombesi, F., Tazaki, F., Mushotzky, R. F., Ueda, Y., Cappi, M., Gofford, J., Reeves, J. N. & Guainazzi, M. 2014, MNRAS, 443, 2154

Walton, D. J., Middleton, M. J., Pinto, C., Fabian, A. C., Bachetti, M., Barret, D., Brightman, M., Fuerst, F., Harrison, F. A., Miller, J. M. & Stern, D. 2016, ApJ, 826, L26